Chapter 2
Analysis on the EMMS Theory

2.1 General

In order to develop an accurate Energy Minimum Multiscale (EMMS) drag model, it is necessary to clarify the effects of mesoscale structure on drag force and identify the key parameter that are decisive to drag. This chapter aims to give the research results of this aspect in three sections. Section 2.1 examines the solving methods and results of cluster characteristic parameters (size and density) and drag function based on a relatively reliable heterogeneous drag model QL-EMMS. Problems within the EMMS theory itself and the reasons behind them are discussed. Section 2.2 focuses on cluster size based on theoretical analysis and physical judgment. Cluster size correlation conforming to physical judgment is introduced into the QL-EMMS model to investigate its effects on drag function. Section 2.3 analyzes the relationship between cluster density and solids concentration. Examine how cluster density acts on drag function and clarify cluster characteristic parameters that are essentially determinative to drag.

2.2 EMMS Theory

As mentioned above, several heterogeneous drag models have been developed from the EMMS theory. They are collectively called "EMMS models." Among them, the QL-EMMS model not only considers the contribution of local solids acceleration, but also discriminates the difference among particle accelerations in dense, dilute, and interaction phases. Besides that, its stress equation treatment for particle in dense phase is more accurate. It is therefore believed to be a relatively reliable EMMS model [1, 2]. The following studies are based on the QL-EMMS model to discuss problems with the EMMS theory itself and the reasons behind them.

C. Chen, *Investigations on Mesoscale Structure in Gas–Solid Fluidization and Heterogeneous Drag Model*, Springer Theses,
DOI 10.1007/978-3-662-48373-2_2

2.2.1 Basic Equations

The key of the Theory of EMMS lies in system decomposition and extreme stability condition. Figure 2.1 gives a vivid description of the mesoscale structure and phase interaction in heterogeneous gas–solid fluidization processes after system decomposition. The entire heterogeneous system is decomposed into three hypothetic uniform subsystems, particle dense phase (cluster), particle dilute phase, and their interaction phase. This gives rise to three scales of phase interaction. The microscale effect is the interaction between gas flow and single particles inside each subsystem. The mesoscale effect is the interaction between the dilute and dense phases resulted from gas flowing round the dense phase. The macroscale effect is the interaction between the entire gas–solid fluidization system and the reactor wall. Clusters between microscale single particles and macroscale reactor are also called "mesoscale structure."

From Fig. 2.1, the state of the entire system can be represented by ten variables: solid content in dilute/dense phase ($\varepsilon_{sf}/\varepsilon_{sc}$), gas velocity in dilute/dense phase (U_f/U_c), particle velocity in dilute/dense phase (U_{pf}/U_{pc}), particle acceleration in dilute/dense phase (a_f/a_c), the volume fraction of dense phase in the entire system (f). Besides, the dense phase is regarded as a cluster and the equivalent cluster size is expressed as d_{cl}. By integrating these variables, we get the state variable representing the entire heterogeneous system, $\vec{X}$

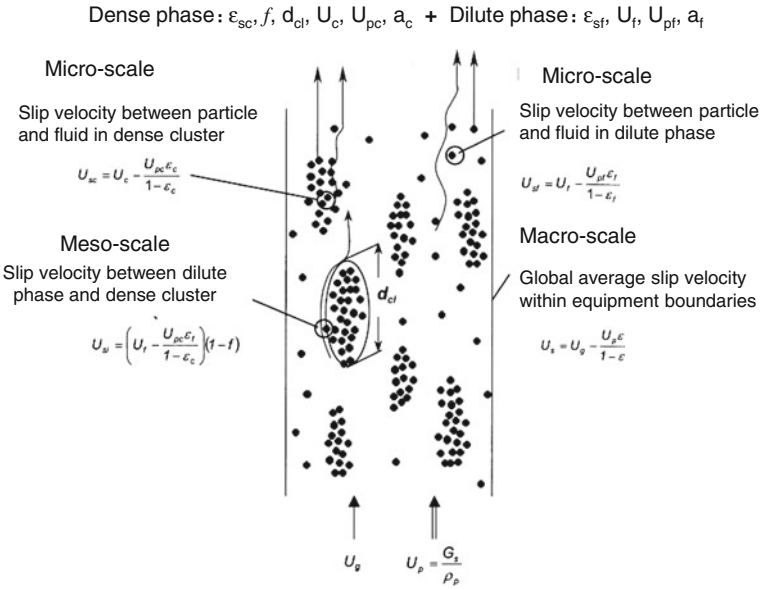

Fig. 2.1 Decomposition of mesoscale structures and phase interaction in heterogeneous gas–solid fluidization system [5]

$$\overrightarrow{X} = \left(\varepsilon_{\mathrm{sc}}, \varepsilon_{\mathrm{sf}}, U_{\mathrm{c}}, U_{\mathrm{f}}, U_{\mathrm{pc}}, U_{\mathrm{pf}}, d_{\mathrm{cl}}, f, a_c, a_f\right) \tag{2.1}$$

where solids concentration in dense phase (cluster) $\varepsilon_{\mathrm{sc}}$ has the following relation with cluster density ρ_{cl},

$$\rho_{\mathrm{cl}} = \rho_{\mathrm{p}} \cdot \varepsilon_{\mathrm{sc}} + \rho_{\mathrm{g}} \cdot (1 - \varepsilon_{\mathrm{sc}}) \tag{2.2}$$

For a given gas and solid particle, the gas and solid densities (ρ_{g} and ρ_{p}) are constant and thus $\varepsilon_{\mathrm{sc}}$ is equivalent to ρ_{p}. To simplify the expression, we will use "cluster density" for "solids concentration in cluster" in the next paragraphs.

Six basic equations including mass conservation equation, force equilibrium equation, and pressure drop equilibrium equation for dilute and dense phases, respectively, plus a cluster size equation, are established to describe the relation among these ten variables.

(1) Particle force equilibrium equation in dense phase per unit volume

$$fn_{\mathrm{c}}F_{\mathrm{c}} + n_{\mathrm{i}}F_{\mathrm{i}} = f\varepsilon_{\mathrm{sc}}\left(\rho_{\mathrm{p}} - \rho_{\mathrm{g}}\right)(g + a_c) \tag{2.3}$$

(2) Particle force equilibrium equation in dilute phase per unit volume

$$n_{\mathrm{f}}F_{\mathrm{f}} = \varepsilon_{\mathrm{sf}}\left(\rho_{\mathrm{p}} - \rho_{\mathrm{g}}\right)(g + a_{\mathrm{f}}) \tag{2.4}$$

(3) Pressure drop equilibrium equation per unit bed height

$$(\Delta p/\Delta h)_f + \frac{(\Delta p/\Delta h)_i}{1-f} = (\Delta p/\Delta h)_{\mathrm{c}} \tag{2.5}$$

$$n_f F_f + \frac{n_i F_i}{1-f} = n_c F_c \tag{2.6}$$

(4) Gas mass conservation equation

$$U_{\mathrm{g}} = U_{\mathrm{f}}(1-f) + U_{\mathrm{c}}f \tag{2.7}$$

(5) Particle mass conservation equation

$$U_{\mathrm{p}} = U_{\mathrm{pf}}(1-f) + U_{\mathrm{pc}}f \tag{2.8}$$

(6) Equivalent cluster size

$$d_{\mathrm{cl}} = \frac{\left[\frac{U_{\mathrm{p}}}{1-\varepsilon_{\max}} - \left(U_{\mathrm{mf}} + \frac{\varepsilon_{\mathrm{mf}}U_{\mathrm{p}}}{1-\varepsilon_{\mathrm{mf}}}\right)\right]g}{N_{\mathrm{st}}\frac{\rho_{\mathrm{p}}}{\rho_{\mathrm{p}}-\rho_{\mathrm{g}}} - \left(U_{\mathrm{mf}} + \frac{\varepsilon_{\mathrm{mf}}U_{\mathrm{p}}}{1-\varepsilon_{\mathrm{mf}}}\right)g} d_{\mathrm{p}} \tag{2.9}$$

where N_{st} is the suspended transport energy defined as the energy consumed by gas to transport unit mass particle in suspension, and equals to the sum of the suspended transport energy of all the subsystems.

$$\begin{aligned} N_{st} &= (N_{st})_c + (N_{st})_f + (N_{st})_i \\ &= \frac{\rho_p - \rho_g}{\rho_p} g \left[U_g - \frac{\varepsilon_{sc} - \varepsilon_{sf}}{1 - \varepsilon_g} f^2 (1 - f) U_f \right] \end{aligned} \tag{2.10}$$

Besides, the EMMS theory assumes that a stability condition exists in a heterogeneous gas–solid fluidization system. That is, the suspended transport energy has reached its minimum. This stability condition is the result of interaction and coordination between "gas control" and "particle control." The former signifies that gas flow always tends to select to flow along the minimum-resistance path. The latter means that particle always tends to maintain the minimum gravity potential energy.

$$N_{st} \rightarrow \min \tag{2.11}$$

2.2.2 Solving Procedure

Mathematically, the ten state variables, six basic equations, and one extreme condition contained in the EMMS theory as discussed above is a problem of constrained nonlinear programming. Classical solutions to this kind of problem include penalty function, feasible direction, and general reduced gradient, which are quite a challenge to numerical solution and difficult to converge. To solve this problem, a series of heterogeneous drag models together with some simplified solution methods were developed.

The earliest EMMS model assumed that particle drag is balanced with effective gravity. That is the particle acceleration a_f and a_c equals 0, which makes a problem of nonlinear programming composed of eight variables, six equations, and one extreme condition. Using general reduced gradient [3], the result shows that, when target function "N_{st} = min" is satisfied, ε_{sc} equals to ε_{smf} and ε_{sf} equals to $1 - \varepsilon_{max}$. Here, ε_{smf} is the minimum fluidization particle concentration and ε_{max} is the maximum voidage where cluster exists. ε_{max} = 0.9997, which is the exact time when cluster disappears and particles are uniformly distributed in gas [4]. Subsequent researchers [5, 6] directly used "$\varepsilon_{sc} = \varepsilon_{smf}$, $\varepsilon_{sf} = 1 - \varepsilon_{max}$" as the simplified stability condition. In this way, the problem of nonlinear programming is transformed into a problem of linear equation group and the remaining six variables are solved with the six basic equations in closed form. Nevertheless, this EMMS model only applies to the overall analysis of fluidized bed since particle acceleration is neglected.

The latest QL-EMMS model does not have any hypothetic or simplified condition and can solve the gas–solid flow parameters in local cells. It is therefore more

logical and reliable. When performing EMMS analysis on local cells, the average solids concentration in grid is the weighted sum of the respective solids concentration of dilute and dense phases,

$$\varepsilon_s = f\varepsilon_{sc} + (1-f)\varepsilon_{sf} \tag{2.12}$$

Given the average solids concentration in grid, this equation can be added into the basic equation group of the EMMS theory as the seventh one.

In other words, the QL-EMMS model is a nonlinear programming problem composed of ten state variables, seven basic equations, and one extreme condition.

The QL-EMMS model assumes that cluster characteristic parameters (size and density) are the main determinants for local drag and conducts two-step EMMS analysis [7].

The first step conducts EMMS analysis on macro operating conditions (operating gas velocity U_g and particle circulating mass flux G_s), traverses cluster density ε_{sc}, cluster size d_{cl}, and particle acceleration in dilute phase a_f, calculate the remaining seven variables with seven basic equations in closed form, and finally obtains the only solution group by minimum energy constraint. The solution includes the correlation of cluster size and density, $d_{cl}(\varepsilon_s)$ and $\varepsilon_{sc}(\varepsilon_s)$.

The second step conducts EMMS analysis on the local flow parameters (gas velocity u_g, particle velocity u_s and solids concentration ε_s) in cells given by computational fluid dynamics (CFD). The cluster size correlation $d_{cl}(\varepsilon_s)$ achieved in Step 1 is used as a substitute for the original size formula (Eq. 2.9). The cluster density correlation $\varepsilon_{sc}(\varepsilon_s)$ achieved in Step 1 is used as a supplementary equation. This is equivalent to correcting one basic equation and supplementing one basic equation. Now still there are ten variables while the number of equations increases to eight. Finally, all the local state variables are derived by traverse solution and extreme constraint.

With all state variables solved, the average drag function in local grid is derived by summing up the weighted drags in the three subsystems. Thus, the average drag coefficient per unit volume, i.e., the drag function β, is obtained.

$$\beta = \frac{\varepsilon_g}{u_{slip}} F_D = \frac{\varepsilon_g}{u_{slip}} \left[f n_c F_c + (1-f) n_f F_f + n_i F_i \right] \tag{2.13}$$

2.2.3 Result Analysis

With a two-step solution, QL-EMMS model combines global operating parameters with local flow parameters. In the numerical simulation of gas–solid fluidization processes, for each computational grid, as long as CFD simulation gives the average flow parameters u_g, u_s, and ε_s, the drag function can be derived from EMMS analysis and then returned to the CFD momentum conservation equation for next step calculation. According to this coupling process, people usually apply the

QL-EMMS model to the numerical simulation of gas–solid flow, and then compare the calculation and experimental results. Nevertheless, CFD numerical calculation often covers the defects intrinsic to drag models.

From the model solving procedure, the cluster size and density resulted from the EMMS analysis in the first step are the input parameters for the second step, thus directly decide the accuracy of the local grid drag function, which in turn is the input parameter for the CFD calculation in the next step. Therefore, the cluster size and density finally decide the accuracy of flow calculation.

From the view of multiscale validation, it should be performed in turn on "mesoscale" cluster characteristics, "grid-scale" drag function, and "system-scale" gas–solid flow characteristics. The accuracy of each scale relies on the accuracy of the previous scale as the prerequisite.

As a result, before applying a drag model to any numerical simulation of gas–solid fluidization, it is necessary to first conduct mesoscale and grid-scale testing. That is to say, the accuracy of cluster characteristic parameters and drag function should be validated before CFD simulation. However, the analyses of QL-EMMS model reveal some problems.

2.2.3.1 Illogical Description of Cluster Characteristic Parameters

As shown in Fig. 2.2a, cluster size presents a unimodal profile, reaching its maximum near the point where solids concentration is 0.45 but being dozens of times of single particle size both at the dilute end and dense end. This does not agree with physical judgment, especially at the dilute end. It is impossible for particles to gather into clusters when solids concentration approaches zero. If any, only a very modest number of particles are scattered in gas flow. So it is impossible for the so-called cluster size to be 50–100 times the single particle size. What's more, no reasonable explanation has ever been given as to why cluster size reaches its maximum at $\varepsilon_s = 0.45$.

The reason why QL-EMMS model gives such a result lies in the defects in its cluster size formula. In the EMMS theory, cluster size is assumed to be inversely related to system suspended transport energy. That is, the larger energy consumption means the smaller cluster size. This formula has been widely doubted and regarded as one of the aspects to be improved within the EMMS theory.

As shown in Fig. 2.2b, cluster density increases monotonously with increasing solids concentration, but suddenly deflects at solids concentration of 0.45, and finally stabilizes at the dense end. In reality, gas–solid fluidization is a varying process in which cluster density should change smoothly and continuously with local solids concentration without any sudden deflection. Further, why cluster density remains constant in a high solids concentration region lacks physical implication.

The reason must be that the EMMS theory lacks an equation describing cluster density which is a traverse solution and minimum energy constraint. Therefore, it is necessary to find other solving method or introduce an accurate, reliable cluster density model.

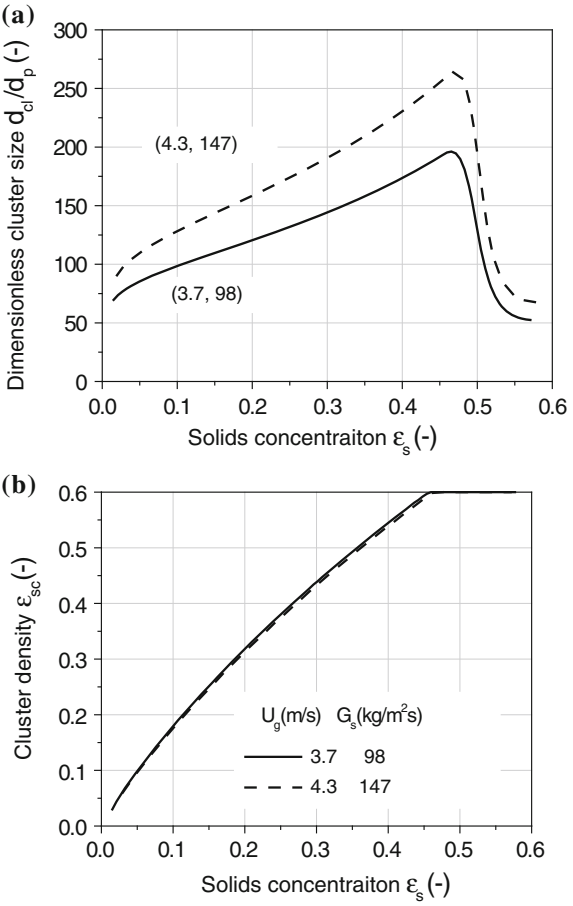

Fig. 2.2 Cluster characteristic parameters predicted by QL-EMMS model (ρ_g = 1.144 kg/m^3, μ_g = 1.848 × 10^{-5} Pa s, ρ_p = 1714 kg/m^3, d_p = 76 μm, ε_{smf} = 0.6). **a** Dimensionless cluster size. **b** Cluster density

2.2.3.2 Inability to Reflect the Essential Feature of Drag Reduction

Figure 2.3 compares the drag functions from the QL-EMMS model, the uniform model, and the O-S model. Compared with the uniform drag function curve, the QL-EMMS can reflect the drag reduction in connection with heterogeneous flow characteristics, but the pattern of reduction does not agree with the experiment-based O-S curve. As shown by the O-S curve, drag function changes continuously and smoothly with local solids concentration, first decreasing, then increasing, and approaching to the uniform curve at the dilute end ($\varepsilon_s \rightarrow 0$) and the dense end ($\varepsilon_s > 0.4$). The QL-EMMS model, on the other side, rises monotonously with local solids concentration and suddenly deflects at $\varepsilon_s = 0.45$, increasing the ascending rate and even exceeding the uniform drag function. The deflection point of drag function corresponds to that of cluster characteristic parameters (Fig. 2.2). This also confirms the importance of cluster characteristic parameters on drag force.

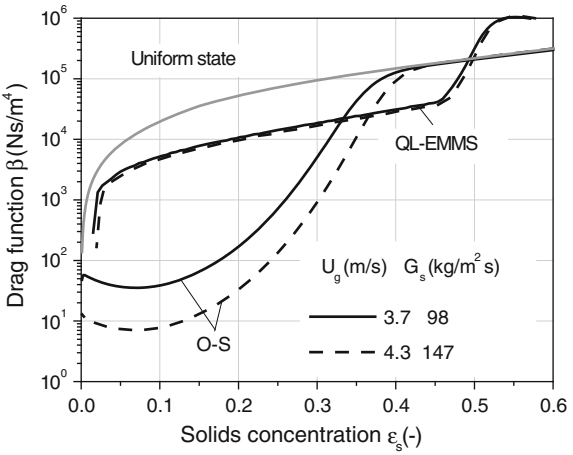

Fig. 2.3 Chart comparing the drag coefficient of QL-EMMS model with uniform model and O-S result (ρ_g = 1.144 kg/m^3, μ_g = 1.848 × 10^{-5} Pa s, ρ_p = 1714 kg/m^3, d_p = 76 μm, ε_{smf} = 0.6)

In a word, although the QL-EMMS model is able to reflect drag reduction in heterogeneous flow, it cannot capture the essential rule of drag reduction.

2.2.3.3 Poor Condition Universality

As shown in Fig. 2.3, the O-S curves under two conditions are nearly one order of magnitude apart from each other, and the drag function is smaller under high particle circulating mass flux G_s. This is because the increase of G_s increases the solids concentration, flow heterogeneity, and thus reduce drag in fluidized bed. Nevertheless, the QL-EMMS drag function curves under two conditions are almost completely overlapped. It cannot capture the effects of condition changes.

This must be related to the cluster characteristic parameters. The cluster density curve in Fig. 2.2b hardly changes with the condition. Though the cluster size in Fig. 2.2a increases with G_s, it does not make much difference to the drag function. This, on the one hand, suggests that cluster size does not increase much and, on the other hand, drag function is not sensitive to cluster size. The possible key factor lies in cluster density. Thus, it is necessary to examine the effects of cluster characteristic parameters on drag function, and identify a parameter that is decisive to drag function. Only this key parameter has the ability to automatically reflect the effect of condition changes, the model can be condition universal.

In order to solve the problems mentioned above, and to improve the EMMS theory, it is necessary to incorporate more equations in addition to improving the existing equations. The EMMS theory contains a number of variables, a limited number of basic equations, and one extreme condition, making it mathematically a problem of constrained nonlinear programming. The constraint function is the basic equation that restricts the range of extremum solution, and the target function is the stability condition that decides the uniqueness of the solution. When the number of basic equations is much smaller than the state parameters, the feasible domain for

extremum solution is too broad to find out the true value definitely although it is mathematically solvable. This is because it is hard for a few constraint equations to tell whether they can fully reflect the true characteristics of a gas–solid fluidization system. The trueness of experimental test solution is the "ultimate" validation, but it does not solve how the true value is obtained.

Therefore, it is important to add as many basic equations as practically possible to reduce the feasible domain and help to obtain the true solution. Meanwhile, basic equations should reflect the real physical processes to the largest extent. That is, basic equations must be both logical and reliable.

The two-step solution of the QL-EMMS model is actually also a process of "improving the existing equations and incorporating more ones." That is, it uses the cluster size from the first step to correct the original cluster size equation, and the cluster density from the first step as a supplementary equation in the second step. As a result, the cluster characteristic size and density results inevitably decide the accuracy of the drag function result. Furthermore, as cluster is the essential source of flow heterogeneity, accurate descriptions of cluster characteristics are absolutely crucial to accurate prediction of heterogeneous drag.

So far, researchers across the globe have highly recognized the importance of cluster size, believing that it makes critical contribution to drag. They believe that developing an accurate cluster size model is an important direction for improving drag models. Yet, few researches have been reported concerning cluster density.

In view of this, this study examines the effects of cluster size and density on drag function respectively, and conduct comparative analysis to identify which is the key decisive factor. This will guide the improvement of the EMMS theory.

2.3 Cluster Size and Its Effects on Drag

In real gas–solid flow processes, clusters appear in varying shapes like flocs, belts, clusters, or flakes and change continuously with time as shown in Fig. 2.4. Hence, cluster size is not always the spherical diameter, but may also indicate its axial or radial length or equivalent diameter. This nonuniform definition makes it difficult to truly compare the size of different shapes of clusters.

Generally, cluster size is measured by fiber photography or double-probe fiber. The results are often limited to the axial size of clusters when they are in vertical movement, but do not reflect their exact horizontal scale. This often gives rise to deviation in understanding.

Existing cluster size models mainly include the empirical model based on experimental measurement, the equivalent diameter model based on simple hypotheses, and the model within the EMMS theory itself (Eq. 2.9), as will be discussed in the next subsection.

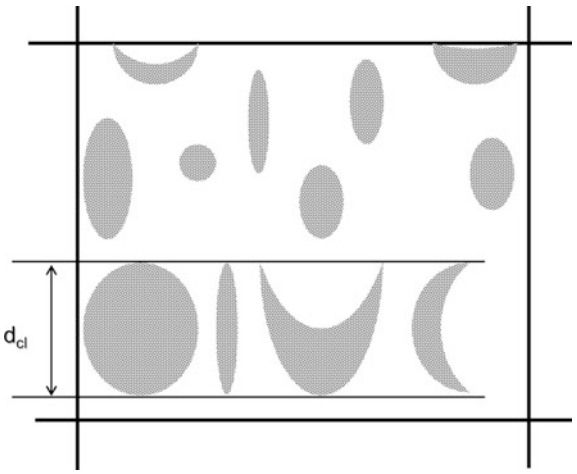

Fig. 2.4 Cluster size by shape

2.3.1 Cluster Size Model

2.3.1.1 Empirical Models and Equivalent Diameter Model

There are a number of empirical formulas describing cluster size [8–10],

$$d_{\mathrm{cl}} = 1 + 1.8543 \cdot \left[(1-\varepsilon_{\mathrm{s}})^{-1.5} \cdot \varepsilon_{\mathrm{s}}^{0.25} / (0.6-\varepsilon_{\mathrm{s}})^{2.41} \right]^{1.3889} \tag{2.14}$$

$$d_{\mathrm{cl}} = d_{\mathrm{p}} + (0.27 - 10 d_{\mathrm{p}}) \varepsilon_{\mathrm{s}} + 32 \varepsilon_{\mathrm{s}}^{6} \tag{2.15}$$

$$d_{\mathrm{cl}} = 1.125 \cdot (1 + 3.8 \cdot (1-\mathrm{ee}) \cdot \mathrm{gg}) \cdot \mu_{\mathrm{g}}^{0.667} \cdot \left(9.8 \cdot \left(1 - \frac{\rho_{\mathrm{g}}}{\rho_{\mathrm{p}}} \right) \right)^{0.333} \tag{2.16}$$

where

$$\mathrm{ee} = 0.6 \cdot \left(1 - (1 - \varepsilon_{\mathrm{s}}/0.6)^{3.4} \right)$$

$$\mathrm{gg} = \frac{1}{1-(\varepsilon_{\mathrm{s}}/0.6)^{0.333}}$$

Figure 2.5 shows the cluster size curves from the empirical formulas above. Their commonplace is that cluster size increases monotonously with local solids concentration and even tends toward infinite. Cluster size is generally several orders of magnitude larger than single particle size. For example, from the "ring-nucleus" structure in fluidized bed, in the near-wall "ring" region where the solids concentration is high and moves down the wall, possibly giving shape to belt-like cluster, thus the measured size is larger. In the "nucleus" region at the center where the flow is quite dilute, the cluster size is naturally smaller.

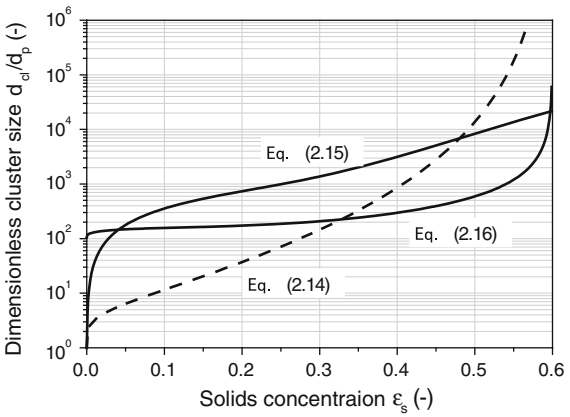

Fig. 2.5 Cluster size versus local solid concentration (ρ_g = 1.144 kg/m^3, $\mu_g = 1.848 \times 10^{-5}$ Pa s, ρ_p = 1714 kg/m^3, d_p = 76 μm)

Some scholars summarized the experimental data of clusters in the near-wall region and worked out the correlation between cluster size and average cross-sectional particle concentration $\varepsilon_{s,av}$ [11],

$$d_{cl} = \frac{\varepsilon_{s,av}}{40.8 - 94.5\varepsilon_{s,av}} \tag{2.17}$$

As shown in Fig. 2.6, the variation of cluster size with average cross-sectional particle concentration is similar to that shown in Fig. 2.5. That means that high solids concentration, whether local or cross-sectional average, is statistically good for cluster expansion, especially in the near-wall region. However, as size is defined and used differently, data in these figures actually contain information of different radial positions and do not truly reflect the internal relation between $d_{cl} \sim \varepsilon_s$. This results in disagreed understanding on d_{cl} and also proves that the cluster size model is not logical, accurate mathematical model either. Of course, the restriction of this model to specific experimental conditions also makes it hardly condition universal.

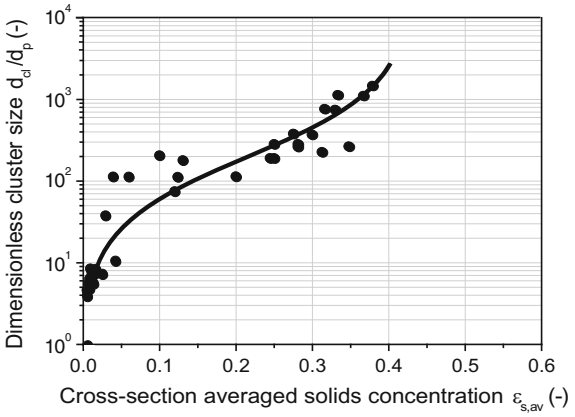

Fig. 2.6 Cluster size versus average cross-sectional particle concentration

One model worthy of notice is the equivalent diameter model based on theoretical analysis [12]. It assumes that a bubble exists at the tail of each cluster in a gas–solid fluidization system, and the volumetric ratio of them equals to the ratio of the dense phase volumetric fraction to dilute phase volumetric fraction,

$$\frac{d_{\mathrm{cl}}^3}{d_v^3} = \frac{f}{1-f} \tag{2.18}$$

where, d_v is the bubble diameter.

Considering that cluster size must be no smaller than single particle size, this formula is written as,

$$d_{\mathrm{cl}} = \left(\frac{f}{1-f}\right)^{1/3} d_v + d_{\mathrm{p}} \tag{2.19}$$

Assuming particles are all in clusters and no particle is contained in the bubble, there is,

$$\varepsilon_{\mathrm{s}} = f\varepsilon_{\mathrm{sc}} \tag{2.20}$$

$$d_{\mathrm{cl}} = \left(\frac{\varepsilon_{\mathrm{s}}}{\varepsilon_{\mathrm{sc}} - \varepsilon_{\mathrm{s}}}\right)^{1/3} d_v + d_{\mathrm{p}} \tag{2.21}$$

Then, introducing the bubble diameter formula, the equivalent diameter formula for clusters is obtained,

$$d_{\mathrm{cl}} = \left(\frac{\varepsilon_{\mathrm{s}}}{\varepsilon_{\mathrm{sc}} - \varepsilon_{\mathrm{s}}}\right)^{1/3} \frac{2u_{\mathrm{t}}^2}{g}\left(1 + \frac{u_{\mathrm{t}}^2}{0.1225(gD)}\right)^{-1} + d_{\mathrm{p}} \tag{2.22}$$

where D is the fluidized bed riser diameter and u_{t} is the single particle terminal velocity.

This model connects d_{cl} to local solids concentration ε_{s}, cluster density $\varepsilon_{\mathrm{sc}}$, particle properties, and fluidized bed size. Technically, it should be able to reflect physical realities. However, as shown in Fig. 2.7, the model curve (assuming $\varepsilon_{\mathrm{sc}}$ is constant and equals to $\varepsilon_{\mathrm{smf}}$) actually gives similar results as other models. Obviously, there are two loopholes in this model. One is that Eq. (2.20) assumes a linear relation, whereas in reality, it is impossible for all particles to come into clusters. The other is that, if Eq. (2.20) applies, the bubble volume should vary with flow. Yet, the d_v formula introduced by Eq. (2.22) only relates to particle terminal velocity and fluidized bed pipe diameter, and constitutes a basically constant parameter. These loopholes decide that d_{cl} can only be inversely related to $(\varepsilon_{sc} - \varepsilon_s)^{1/3}$ and present monotonous variation.

Analyzing this result from the equivalence between cluster and flow heterogeneity, there will be a conflict. As well known, a larger cluster size signifies a higher

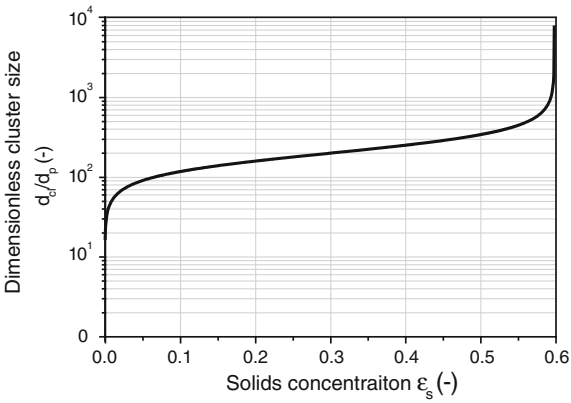

Fig. 2.7 Resulting equivalent cluster diameter (ρ_g = 1.144 kg/m^3, μ_g = 1.848 × 10^{-5} Pa s, ρ_p = 1714 kg/m^3, d_p = 76 μm, ε_{smf} = 0.6, D = 305 mm)

level of flow heterogeneity. When flow tends toward dilute, this is understandable. But when flow tends toward dense end, the flow should tend to be uniform, and the solids concentration at different spatial points should tend toward consistent. Obviously, the results in Figs. 2.5, 2.6, 2.7 disagree with this physical analysis.

Furthermore, from the perspective of drag, as can be seen from Fig. 1.2, drag function gradually returns to a uniform state value with increasing solids concentration. This suggests that mesoscale effect at extremely large solids concentration should gradually disappear and no cluster exists. Hence, the cluster size should be equal to the particle size. Then why the fact that very large cluster size is read in the high solids concentration in experiments? The only explanation is that the so-called "size" measured in experiment is actually the vertical length between the measurement discontinuity points.

If we directly apply this model to numerical simulation without analysis or judgment, we will discover that the cluster size is not only far larger than the grid size, but also even exceed the device size. In such case, if we try to correct drag with such a size parameter, we will find ourselves troubled by these conflicts.

Based on the analysis above, it is believed that the essential source of all these conflicts is the fact that, up to date, the variation of cluster size d_{cl} in a dense region has never been clarified. As such, it is necessary to further examine the stress condition during particle clustering.

First, the accurate cluster definition in its traditional sense must be identified. According to the definition in Horio et al., a cluster is the particle collection formed under gas flow, represented by spatial heterogeneous distribution of solids concentration [13, 14]. Once a cluster takes form, it will immediately change the local flow condition and result in resistance to gas flow. Gas naturally selects to flow toward a more dilute area, i.e., where the resistance is smaller, around the cluster, rather than through the cluster. This leads to a velocity slip that is much larger than single particle velocity between the falling particles and the gas flow. In other words, the drag on the cluster as a whole is far smaller than that on single particles,

what we call drag reduction. If we take clusters as a loose large particle, it will be easier to understand this phenomenon.

Second, the formation of clusters relies on particle and gas flow conditions. Only when there are a sufficient number of particles (ε_s) in space with room for free movement (free path), can cluster forms under gas flow entrainment. The maximum level of this cluster formation is the accumulation state, which is generally the minimum fluidization solids concentration ε_{smf}.

Furthermore, during particles collection, intensive collision and friction takes place between particles, between particles and clusters, and between clusters, which also cause clusters to break up and even dissipate the next moment. Hence, in fluidization process, forces boosting clusters (gas flow) and degrading clusters (collision and friction) both exist.

Obviously, in dense flows ($\varepsilon_s > 0.2$), as solids concentration increases, the free path gradually reduces and the collision effect degrades while the friction effect gradually intensifies and becomes a constraint on flow and an obstacle to particle movement. The gradual increase of flow resistance continues to degrade the driving effect of gas flow. In this way, the cluster is impeded and gradually degrades and disappears. In other words, the cluster size should tend to reduce. When ε_s is close to ε_{smf}, there will be no room for particles to move freely, and it will be impossible for them to come into clusters. This results in uniform flow typically in the form of particle flow. As a result, the cluster size d_{cl} should eventually tends toward single particle size d_p. The conflicts mentioned above are readily solved.

The reason why experiments gave those unreasonable results lies in the inconsistent definition of cluster size. As discussed above, in the near-wall region of fluidized bed, almost continuous particle descending flow is formed. The measurement taken at this time is simply not the cluster size in its true sense. In reality, in the vertical flow of fluidization, similar to single particle deposition, the key size deciding cluster movement is not its axial length, but rather, its cross-sectional size. As solids concentration increases, the cluster is already broken into a very small size by friction. This explains why results from the models are physically inconsistent. They can neither help to achieve a deeper understanding of mesoscale effect, nor be used as a mathematical model to correct drag.

2.3.1.2 Correction Model Based on EMMS Theory

Look back on the previously mentioned O-S drag model [15]. In Eq. (1.7), the second term of heterogeneous coefficient f_c is precisely the heterogeneous correction term. The remaining part other than empirical coefficient C_3 is actually a unimodal function. It is right that this term decides the unimodal profile of the heterogeneous drag curve in O-S model.

As analysis stated above, the cluster size given by the latest QL-EMMS drag model (Eq. (2.9) and Fig. 2.2a) does not conform to physical understanding. Hence, Eq. (2.9) is corrected with the unimodal function form in f_c, i.e., Eq. (2.23), and obtained Eq. (2.24) [1].

$$f_{\mathrm{cl}} = Re\,\varepsilon_{\mathrm{s}} \mathrm{e}^{-0.005(Re-5)^2-90(0.08-\varepsilon_s)^2} \tag{2.23}$$

$$d_{\mathrm{cl}} = \left\{ \frac{f_{\mathrm{cl}}}{f_{\mathrm{cl,max}}} \cdot \frac{\left[\frac{U_{\mathrm{p}}}{1-\varepsilon_{\mathrm{max}}} - \left(U_{\mathrm{mf}} + \frac{\varepsilon_{\mathrm{mf}} U_{\mathrm{p}}}{1-\varepsilon_{\mathrm{mf}}}\right)\right] g}{N_{\mathrm{st}} \frac{\rho_{\mathrm{p}}}{\rho_{\mathrm{p}}-\rho_{\mathrm{g}}} - \left(U_{\mathrm{mf}} + \frac{\varepsilon_{\mathrm{mf}} U_{\mathrm{p}}}{1-\varepsilon_{\mathrm{mf}}}\right) g} + 1 \right\} \cdot d_{\mathrm{p}} \tag{2.24}$$

The cluster sizes before and after model correction are shown in Fig. 2.8.

As shown in Fig. 2.8, the corrected cluster size also presents a unimodal profile. The peak value is moved from the original $\varepsilon_{\mathrm{s}} = 0.45$ to nearby 0.1. The value is slightly descended. At the $\varepsilon_{\mathrm{s}} \rightarrow 0$ dilute end and $\varepsilon_{\mathrm{s}} \rightarrow 0.6$ dense ends, d_{cl} tends toward single particle diameter, $d_{\mathrm{cl}}/d_{\mathrm{p}} \rightarrow 1$. This conforms to the physical reality and our previous analysis.

Further studies are still needed to find out what difference this correction will make to drag. The result is given below.

To ensure the comparability, the condition for subsequent calculations is unified as, $\rho_{\mathrm{g}} = 1.144$ kg/m^3, $\mu_{\mathrm{g}} = 1.848 \times 10^{-5}$ Pa s, $\rho_{\mathrm{p}} = 1714$ kg/m^3, $d_{\mathrm{p}} = 76$ μm, $\varepsilon_{\mathrm{smf}} = 0.6$, $U_{\mathrm{g}} = 3.7$ m/s, $G_{\mathrm{s}} = 98$ kg/m^2 s.

2.3.2 *Effects on Drag*

Figure 2.9 shows that, both cluster density $\varepsilon_{\mathrm{sc}}$ and drag function β significantly changed, after introducing the corrected cluster size into the QL-EMMS drag model.

The overall shape of cluster density $\varepsilon_{\mathrm{sc}}$ stays the same, except that the deflection point moves forward from the original $\varepsilon_{\mathrm{s}} = 0.45$ to nearby 0.3. Some important changes take place in drag functions.

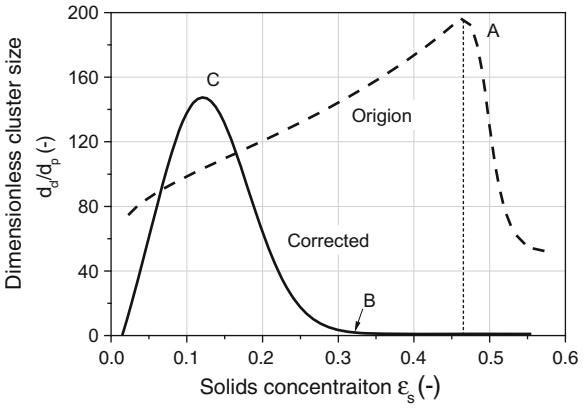

Fig. 2.8 Cluster size before and after model correction ($\rho_{\mathrm{g}} = 1.144$ kg/m^3, $\mu_{\mathrm{g}} = 1.848 \times 10^{-5}$ Pa s, $\rho_{\mathrm{p}} = 1714$ kg/m^3, $d_{\mathrm{p}} = 76$ μm, $\varepsilon_{\mathrm{smf}} = 0.6$, $U_{\mathrm{g}} = 3.7$ m/s, $G_{\mathrm{s}} = 98$ kg/m^2 s)

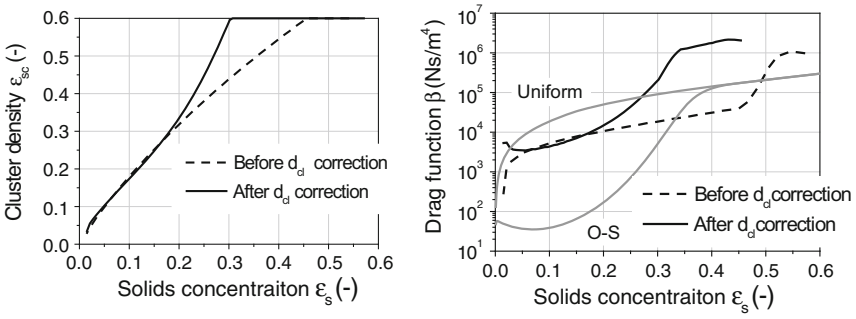

Fig. 2.9 Effects of cluster size correction. **a** Cluster density. **b** Drag function

(1) The overall shape presents concave function with characteristics similar to O-S model, and the minimum value also appears nearby the solids concentrate where the maximum d_{cl} is located, suggesting that the corrected cluster size distribution does reflect the characteristics of heterogeneous flow.

(2) Drag function rises about two orders of magnitude within $\varepsilon_s = 0.2–0.6$, which is obviously the reflection of the divergence before and after d_{cl} within the same range. But the drag function is larger than that of uniform flow, which has no physical significance.

(3) The deflection point of the drag function curve before and after correction corresponds in position to the d_{cl} curve. That is respectively the maximum positions of the d_{cl} curve before correction (point A in Fig. 2.8), and the transition from a unimodal curve toward a horizontal one after correction (point B). After point B, d_{cl} tends toward d_p, implying that cluster gradually disappears and flow tends toward uniform. Drag function also presents this change. That is, like the O-S curve, its ascending tendency gradually disappears and tends toward gentle after the deflection point. Besides, the convex and concave character of the d_{cl} curve at points A and B are precisely inverted in the drag function curve into concave and convex character. Further observation on the curve within $\varepsilon_s = 0–0.3$ also discovers this "specular" correspondence. Before correction, d_{cl} curve is close to a straight linear and the drag curve is similar. After correction, it becomes a convex function at $\varepsilon_s = 0.13$ (point C), and at the same position the drag curve becomes a concave function. This is right the change we discussed in article (1).

(4) From another perspective, the drag curve after the d_{cl} correction looks very much like the result of moving the O-S model curve laterally upwards. We cannot help to wonder if this lateral movement implies that the absolute cluster size after correction is too small, and this explains why the drag reduction is not as significant as the O-S curve. Further, to remove the nonphysical character of the curve after $\varepsilon_s > 0.3$ beyond the uniform value, what we need to do seems to be simply cause the gentle part to overlap the uniform curve. This reminds us the necessity to further examine what difference the absolute d_{cl} value makes to drag.

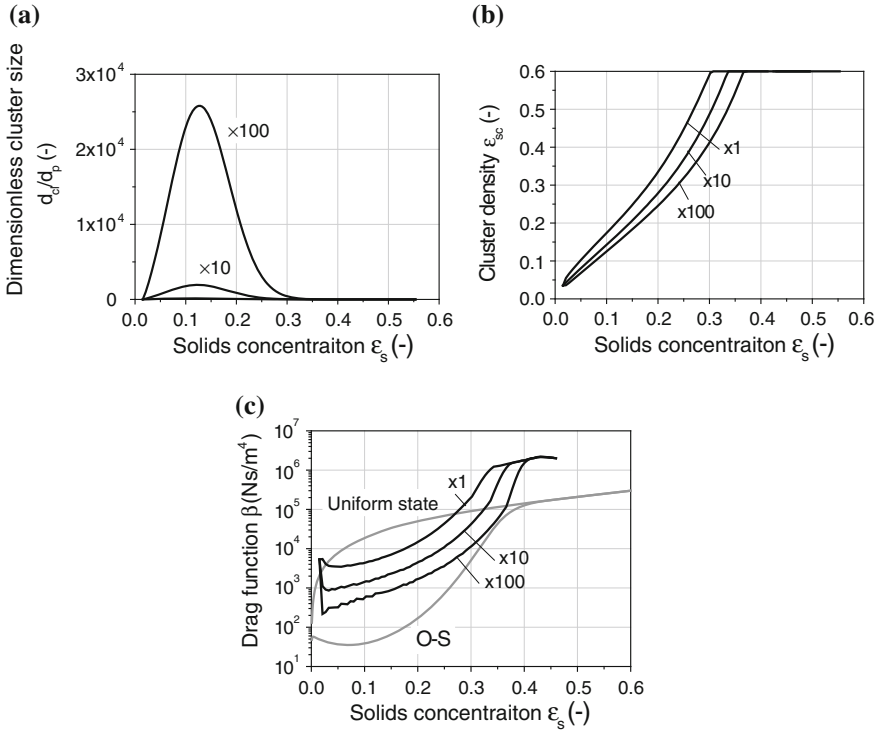

Fig. 2.10 Effects of increasing cluster size. **a** Dimensionless cluster size. **b** Cluster density. **c** Drag function

Thus, we directly multiply d_{cl} Eq. (2.24) with 10 and 100 and keep the size distribution unchanged. The results are shown in Fig. 2.10.

Figure 2.10 shows that, when cluster size is amplified, both cluster density and drag function reduce, but no "lateral movement" appears as expected. Instead, the drag function curve is gradually distorted, gradually becoming more divergent from the O-S curve, and appears to be less sensitive. At $\varepsilon_s = 0.1$, though d_{cl} is already 10^4 times of d_p, the β value is still one order of magnitude higher than O-S model. After $\varepsilon_s > 0.3$, the curve still exceeds the uniform flow values, except that the deflection point has slightly moved toward the dense region. This is because d_{cl} has remained close to d_p within this range.

Therefore, unlike what was previously assumed that d_{cl} is the principal and only factor contributor to mesoscale effect and drag reduction, relying on it alone is not enough to provide accurate heterogeneous drag. It can be inferred that there is definitely another factor that makes a substantial difference to drag. Hence, it is necessary to examine the contribution made by the other cluster characteristic parameter, the cluster density.

2.4 Cluster Density and Its Effects on Drag

The EMMS theory provides no formula that solves ε_{sc} directly, but uses the "traverse" algorithm and minimum energy constraint. Therefore, it is in an "enslaved" driven position. This also mirrors the deficiencies of current research and the lack of understanding of this problem.

As shown in Figs. 2.2, 2.9, and 2.10, the variation of ε_{sc} with solids concentration is virtually sublinear monotonous rise, followed by a deflection, before stabilizing at ε_{smf}. Some author directly assumed that it constantly equals to the minimum fluidization solids concentration, $\varepsilon_{sc} = \varepsilon_{smf}$, which cannot be supported by substantial research basis [16].

In view of this, it is necessary to study the variation of cluster density with solids concentration and its effects on drag.

2.4.1 Empirical Formula for Cluster Density

The following equations are empirical cluster density formulas from regressing experimental data. The only difference is that Eq. (2.25) uses the cross-sectional average solids concentration $\varepsilon_{s,av}$ [11], while the other two use the local solids concentration ε_s [17, 18].

$$\varepsilon_{sc} = \frac{0.58\varepsilon_{s,av}^{1.48}}{0.013 + \varepsilon_{s,av}^{1.48}} \quad 0 < \varepsilon_{s,av} < 0.55 \tag{2.25}$$

$$\varepsilon_{sc} = 0.389 - \frac{0.385}{1 + 66.451\varepsilon_s^{1.536}} \quad 0 < \varepsilon_s < 0.35 \tag{2.26}$$

$$\varepsilon_{sc} = \frac{0.595\varepsilon_s^{1.143}}{0.165 + \varepsilon_s^{1.143}} \quad 0 < \varepsilon_s < 0.4 \tag{2.27}$$

Due to experimental and measurement limitations, no experimental data is available in dense regions where solids concentration is large. All these empirical formulas only apply to a limited range of solids concentration.

Figure 2.11 compares the cluster densities from the empirical formulas and from the QL-EMMS model. All the three formulas provide similar nonlinear monotonous rise with smooth curve. This again indicates that the straight line plus deflection point given by the QL-EMMS model is not reasonable.

Besides, the divergence among the three formulas shows close correlation between ε_{sc} and the experimental condition. That is to say, flows under different conditions have different levels of heterogeneity and result in different mesoscale structures. As a characteristic parameter of mesoscale structure, ε_{sc} will definitely

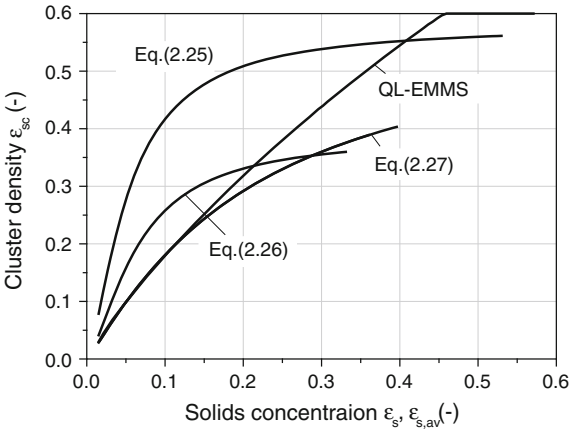

Fig. 2.11 Comparision of cluster density formula and QL-EMMS model result

change with it. Thus, cluster density should be condition-dependent which cannot be represented by the EMMS theory (Fig. 2.2b).

2.4.2 *Effects on Drag*

Of these three empirical formulas discussed above, the latter two agree with the definition in the EMMS theory. That is, they describe the relation between cluster density and local solids concentration. Hence, we can introduce them into the QL-EMMS drag model for calculation and analysis.

Figure 2.12 presents the resulting drag functions under different cluster densities, including the cluster densities from empirical formulas (2.26), (2.27) and from the original "traverse" method. In all these results, cluster size is calculated on the correction model based on the EMMS theory Eq. (2.24).

In Fig. 2.12, after introducing the empirical formula, the resulting drag function immediately presents the essential characteristics of the O-S curve. This is because the curves of ε_{sc} empirical formulas present a convex function shape. However, drag function has no solution in the $\varepsilon_s > 0.3$ dense region, since empirical formulas only apply to a limited range of solids concentration.

Comparing the two ε_{sc} empirical curves, the ε_{sc} from Eq. (2.26) is marginally larger while β is significantly smaller, suggesting that drag function is inversely related to cluster density. Again at $\varepsilon_s = 0.1$, ε_{sc} has increased by approximately 66 %, and this causes β to reduce by one order of magnitude, suggesting that drag function is much more sensitive to cluster density than it is to cluster size d_{cl} (compared with Fig. 2.10).

Comparing the ε_{sc} from empirical formulas and from "traverse" method, the reduction of ε_{sc} at $\varepsilon_s = 0.3$ causes the drag function move downward substantially. This is unachievable by changing d_{cl} as discussed above. Now, looking back on the

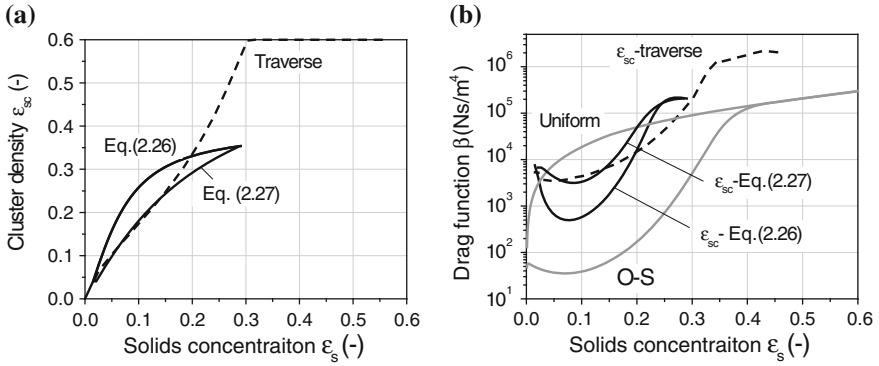

Fig. 2.12 QL-EMMS model results using various cluster density model. **a** Cluster density. **b** Drag function

downward movement of the drag curve in Fig. 2.10c, one will immediately realize that this is not the direct result of changing d_{cl}, but rather, the indirect result of reducing cluster density (Fig. 2.10b).

Analysis above confirms again that the cluster density makes essential difference to drag function. Thus, it is necessary to establish a logical, accurate cluster density model, and introduce it into the EMMS theory as a new equation. This will refine this theory and obtain a drag function that qualitatively and quantitatively agrees with the O-S curve.

2.5 Summary

(1) Through analysis on the QL-EMMS drag model, revealed defects of the EMMS theory in describing cluster characteristics as its equations are not closed. It is identified that the direction for further refining this theory is to establish a new mesoscale (cluster) theoretical model.
(2) Clarified the fuzzy understanding on cluster variation in dense gas–solid two-phase flow and clearly pointed out that, cluster will break up and eventually return to single particle state at extremely dense region. It is identified that the cluster size is unimodally distributed and tends toward single particle size at the dilute and dense ends.
(3) Discovered that drag function is inversely related to cluster size, while it is hardly possible to improve the drag function result simply by changing cluster size.
(4) Cluster size makes a great difference to and is inversely related to drag function. It is necessary to establish a logical, accurate cluster size density to replace the "traverse" solution pattern in the EMMS theory.

References

1. Li F (2009) Investigations on the turbulent gas–solid two-phase interactions in fluidized desulfurization process. Doctoral dissertation, Tsinghua University, Beijing
2. Li F, Chen C, Wang J, Qi H (2011) QL-EMMS drag model and its revision for fluidized dense gas–solid two-phase flow. J Eng Thermophys 1:75–79
3. Li J (1987) Multiscale model for two-phase flow and energy minimum method. Doctoral, The Chinese Academy of Sciences, Beijing (in Chinese)
4. Matsen JM (1982) Mechanisms of choking and entrainment. Powder Technol 32(1):21–33
5. Li JH, Cheng C, Zhang Z et al (1999) The EMMS model-its application, development and updated concepts. Chem Eng Sci 54(22):5409–5425
6. Xu GW, Li JH (1998) Analytical solution of the energy-minimization multi-scale model for gas–solid two-phase flow. Chem Eng Sci 53(7):1349–1366
7. Wang W, Li JH (2007) Simulation of gas–solid two-phase flow by a multi-scale CFD approach—extension of the EMMS model to the sub-grid level. Chem Eng Sci 62(1–2): 208–231
8. Bin Zou, Hongzhong Li, Yashen Xia, Kwauk Mooson (1993) Statistic model for cluster size distribution in fast fluidized bed. Eng Chem Metall 14(1):36–42
9. Gu WK, Chen JC (1998) A model for solid concentration in circulating fluidized beds. In: Fluidization IX, Durango, Colorado, 1998, pp 501–508
10. Gu WK (1999) Diameter of catalyst clusters in FCC. AIChE Symp Ser 95(321):42–47
11. Harris AT, Davidson JF, Thorpe RB (2002) The prediction of particle cluster properties in the near wall region of a vertical riser. Powder Technol 127(2):128–143
12. Subbarao D (2010) A model for cluster size in risers. Powder Technol 199(1):48–54
13. Qi HY (1997) Euler/Euler Simulation der Fluiddynamik Zirkulierender Wirbelschichten. Aachen, Germany: Verlag Mainz, Wissenschaftsverlag. ISBN 3-89653-224-3
14. Horio M, Kuroki H (1994) Three-dimensional flow visualization of dilute dispersed solids in bubbling and circulating fluidized beds. Chem Eng Sci 49(15):2413–2421
15. O'Brien TJ, Syamlal M (1993) Particle cluster effects in the numerical simulation of a circulating fluidized bed. In: Avidan AA (ed) Preprint volume for CFB-IV. AIChE, New York, pp 430–435
16. Naren PR, Lali AM, Ranade VV (2007) Evaluating EMMS model for simulating high solid flux risers. Chem Eng Res Des 85(A8):1188–1202
17. Manyele SV, Parssinen JH, Zhu JX (2002) Characterizing particle aggregates in a high-density and high-flux CFB riser. Chem Eng J 88(1–3):151–161
18. Yang TY, Leu LP (2009) Multiresolution analysis on identification and dynamics of clusters in a circulating fluidized bed. AIChE J 55(3):612–629

http://www.springer.com/978-3-662-48371-8

Investigations on Mesoscale Structure in Gas–Solid Fluidization and Heterogeneous Drag Model

Chen, C.

2016, XVII, 118 p., Hardcover
ISBN: 978-3-662-48371-8